Battery and Supercapacitor Materials in Flow Cells. Electrochemical Energy Storage in a $LiFePO_4$ / Reduced Graphene Oxide Aqueous Nanofluid

*Zahilia Cabán-Huertas[1], Daniel Rueda-Garcia[1], Sergi Sanchez-Ribot[1], Carlos Marchante,[1] Raul Benages,[1] Deepak P. Dubal[2], Omar Ayyad[3], Pedro Gómez-Romero[1]**

1Catalan Institute of Nanoscience and Nanotechnology (ICN2), CSIC and The Barcelona Institute of Science and Technology, Campus UAB, Bellaterra, 08193 Barcelona, Spain

2 School of Chemical Engineering, Engineering North Building, The University of Adelaide, SA 5005, Australia

3Faculty of Engineering, Dept. of Materials Engineering, Al-Quds University, P.O. Box 20002, East Jerusalem, Palestine.

CORRESPONDING AUTHOR FOOTNOTE

Prof. Pedro Gómez-Romero

Tel.: +349373609/+345929950 Fax: +345929951

E-mail: pedro.gomez@icn2.cat (Pedro Gómez-Romero)

Abstract

Exploring conceptual frontiers between batteries, supercapacitors, redox flow batteries (RFBs) and fuel cells (FCs), we have used a battery material (i.e. $LiFePO_4$) and a supercapacitor material (i.e. graphene) in the form of nanoparticles dispersed in an aqueous electrolyte to characterize the electrochemical activity of the resulting electroactive nanofluids.

X-ray diffraction, TEM, Raman, XPS and AFM analyses were carried out to characterize the solid $LiFePO_4$ and RGO components. The corresponding electroactive nanofluids were prepared by dispersion in an aqueous Li_2SO_4 electrolyte and stabilized with DiaminoBenzoic Acid (DABA). Cyclic voltammetry measurements were used to analyze their electrochemical behavior in three-electrode cells. Charge-discharge tests of the $LiFePO_4$/RGO (positive) vs. RGO (negative) nanofluids were also performed. Effective utilization of dispersed electroactive particles (ca. 100 mAh/g(LFP) at 1C) was demonstrated, which turned out to be superior to the same LFP material used as solid electrode. A charge-transfer percolation effect provided by the RGO dispersion is proposed as the mechanism for the good performance of $LiFePO_4$ (not coated with carbon!) and RGO Nanofluids. Our results constitute a first step and proof of concept of the possible application of electroactive nanofluid electrodes in alternative flow batteries.

1 A brief introductory review on the twilight between solid and liquid electroactive materials.

Electrochemical Energy Storage is the midst of a regenerative resurgence. Batteries, SuperCapacitors (SCs), Fuel Cells (FCs) or Redox Flow Batteries (RFBs) are markedly complementary technologies and are all called to play a role within the forthcoming sustainable energy model. From load-leveling devices to wearable electronics, to the development of smart grids to electric vehicles or to renewable energy storage. Exploring conceptual frontiers between batteries, supercapacitors, redox flow batteries (RFBs) and fuel cells (FCs) could provide new opportunities to get the best of each of those technologies.

Redox Flow Batteries (RFBs) for instance could indeed be considered as laying halfway between conventional solid-electrode batteries and FCs. Unlike traditional batteries, energy density and power density are effectively detached in RFBs. Energy is proportional to the size of the external reservoirs and power to the number of cells and area of the electrodes. This technology does not suffer memory effect and benefits from a long cycle life. These are important advantages related to the fact that active materials are ions solvated in the flowing electrolyte media. On the other hand, RFBs have drawbacks like low energy density and low specific energy due to the solubility limit of the active redox species.

All-Vanadium cells for example constitute the most developed type of RFBs and have an energy density of 40 $Wh \cdot L^{-1}$ and a specific energy of 25 $Wh \cdot Kg^{-1}$ and operate between 1.6V and 1.3V.[1, 2] Those values are far away from current Li-Ion Batteries (LIBs), 150-200 $Wh \cdot Kg^{-1}$ at 3.7V.[3]

The primary reason why RFBs do not achieve the energy density values of LIBs is because they suffer from a low concentration of active material due to limited solubility. But in addition, voltages are relatively low due to both thermodynamic and kinetic factors (high internal resistance associated to electrolyte diffusion through selective membrane separators), all of which result in reduced power density.

The recent proposal of Semisolid Flow Batteries (SFBs) tries to solve these drawbacks by using heterogeneous mixtures of electroactive species with surfactant and carbon particles. For example, Chiang and coworkers described a so-called semi-solid lithium flow battery.[4] And Gogotsi and coworkers described a similar system for a capacitive system.[5] A flowable carbon-electrolyte mixture is employed as the active material for capacitive energy storage, and is handled in a similar fashion to flow or semi-solid batteries**.** In 2014, Nair and collaborators also reported a flow capacitor device based on a graphene dispersion in organic electrolyte, with improved energy density (14.3 $W \cdot h \cdot L^{-1}$) with respect to graphite (0.422 $W \cdot h \cdot L^{-1}$).[6] 3D interconnected hybrid materials (rGO@CS) were used to prepare an EFC. When tested as flowable electrodes, the composition with a 1:2 ratio of GO to CS exhibited the highest capacitance of 200 $F \cdot g^{-1}$ and an improved rate performance.[7]

More recently, Tarascon et al. focused on the performance of the $LiFePO_4$/$LiPF_6$ EC-DMC/Li redox flowable half cell. As a result, power density performances greater than 328 $mW \cdot cm^{-2}$ at 104 $mA \cdot cm^{-2}$ were achieved with specific energy of 50 $Wh \cdot kg^{-1}$. It is important to mention, however the use of intermittent flow conditions with the values reported being measured under static conditions.[8]

SFBs usually need a significant amount of dispersed conducting particles such as carbon particles, which can transform the electrolyte solution into a slurry electrode that allows for electrical conduction by percolation in all the volume of the electrode. [5] On the other hand, these conducting particles often need a surfactant to generate a stable dispersion.[9] This large amount of carbon particles and the use of surfactant are responsible for a detrimental increase in the viscosity of semisolid electrodes. Finally, the nature of the carbon used is another crucial point since it determines the electrical conductivity and thus the percolation effect.[10, 11]

High viscosity is not compatible with flow cells, which need a pumping system to flow the solutions from the reservoirs to the electrochemical cell and vice versa, with a corresponding decrease in overall efficiency. Thus, a significant increase in viscosity of the fluids is highly undesirable, because the extra energy needed to circulate the pastes could cancel out the possible intrinsic advantages of the active materials, or at least reduce dramatically the overall efficiency of the system.

A procedure described as “intermittent flow” was used that allowed the slurry to rest on the electrodes prior and during measurements. Under those conditions the process of cycling of the active material could be closer to that of a solid battery electrode rather than to a flowing one.

On the other hand, a different approach to the harnessing of electroactive solid particles in flow cells has been proposed by Grätzel and collaborators by introducing the concept of shuttle redox molecular solutions with suitable redox potentials, solubility, stability and kinetics to transfer the charge to solid particles stored in a separate reservoir.[12]

Other approach using nanofluids was proposed by Timofeeva in 2015. They developed a scalable one-step surface modification procedure for functionalizing TiO_2 nanoparticles with a monolayer coverage of propyl sulfonate groups.[13] This new formulation the nanofluids has a high solid loading and low viscosity, while retaining the surface activity of nanoparticles.

Our approach has been to use graphene instead of activated carbon as the key material to provide an electrical percolation effect on the solution. Thus, a stabilized dispersion of RGO in aqueous sulfuric acid solution can deliver energy storage capacities similar to those of solid electrode supercapacitors (169 $F \cdot g^{-1}$(RGO)) but working up to much faster rates (from 1 $mV \cdot s^{-1}$ to the highest scan rate of 10 $V \cdot s^{-1}$) in nanofluids.[14]

Indeed, RGO must be properly dispersed in electrolytes in order to be used as a nanofluid. This has been attempted both in aqueous and organic solvents. For example Xu et al. reported a successful production of stable high-concentration graphene dispersions in low-boiling-point, low-polarity conventional organic solvents by liquid-phase noncovalent exfoliation of graphite assisted using polyethylene (HDPE) as the stabilizer.[15] Other example of RGO dispersion, this time in water, is the report of an imidazolium-modified hexa-*peri*-hexabenzocoronene derivative (HBC-C_{11}-MIM[Cl^-]) designed and synthesized as a stabilizer to disperse RGO. The resulting RGO/HBC-C_{11}-MIM[Cl^-] hybrid can reach stable concentrations of 5.0 $mg \cdot mL^{-1}$ (RGO) in water.[16] In these two examples the stabilization of the RGO is achieved by a solvated aromatic molecule that keeps RGO in suspension.

On the other hand, $LiFePO_4$ has been intensely studied as cathode material for LIBs since the seminal work of Goodenough in 1997.[17] It has made it from the labs to the market thanks to

its low cost, abundant raw materials, safety, low toxicity, structural stability and excellent electrochemical properties. The active material can be reversibly charged and discharged with a stable voltage profile at 3.45 V vs. Li^+/Li with a very small change in unit cell parameters during the $LiFePO_4/FePO_4$ phase transition. It needs, however, conducting additives and coatings in order to display its full potential. As part of the extensive research done with $LiFePO_4$ Bonaccorso, report a battery with a graphene and $LiFePO_4$ electrodes and an energy density of 190 $Wh \cdot Kg^{-1}$.[18]

In this work, we have used 3,4-diaminobenzoic acid (DABA) to generate a stable RGO dispersion in water and lithium iron phosphate ($LiFePO_4$) nanoparticles with a 2D layered morphology to demonstrate the high rate of charge transfer throughout the graphene dispersion in low concentration and in the absence of conventional surfactants. Just small amounts of RGO dispersed in aqueous Li_2SO_4 electrolyte lead to nanofluids with low viscosity while allowing effective charge/discharge of redox $LiFePO_4$ nanoparticles.

2 Experimental Section

2.1 $LiFePO_4$ Synthesis

$LiFePO_4$ sample was prepared by a reflux method. Stoichiometric amounts (0.03 mmol) of $Li(CH_3COO) \cdot 2H_2O$ (3.0606 g), $Fe(CO_2CO_2) \cdot 2H_2O$ (5.3907 g) and 85 %v/v H_3PO_4 (2.05 mL) were dissolved in 70 mL of ethylene glycol. The liquid reaction mixture was placed in a round-bottom flask connected to a condenser and refluxed vigorously for 72 h at 200 °C. The final pH of this solution was 7. The resulting solid was filtered-off, washed several times with deionized water and then ethanol. The sample was dried under vacuum at 80°C overnight, preheated at

350°C for 5 h and then sintered at 700°C for 10 h under nitrogen atmosphere. We collected 3.4214 g of green powder which amounts to 92% yield.

2.2 RGO synthesis

Graphite oxide (GO) was prepared from natural graphite using a modified Hummers method as follows[19]: $NaNO_3$ (5g) and H_2SO_4 (225mL) were added to graphite (5g) and stirred for 30 min in an ice bath. $KMnO_4$ (25g) was added to the resulting solution, and then the solution was stirred at 50°C for 2 h. Deionized (DI) water (500 mL) and H_2O_2 (30 mL, 35%) were then slowly added to the solution, which was then washed with HCl (750 mL, 10%). Additional washing with concentrated HCl (500 mL, 37%), followed by dialysis for one week and a final drying under vacuum at 70°C, afforded the GO product as a powder. The amount of powder recovered was 4.1381g, which is the 16% yield. Reduced graphene oxide (RGO) was prepared by high temperature treatment of this GO sample at 800°C under N_2 atmosphere for 1 hour.

2.3 Electroactive Nanofluids preparation

The electroactive nanofluids discussed in this article were prepared using 1M solutions of $Li_2SO_4{\cdot}H_2O$ as base fluid and different DABA concentrations. RGO was then dispersed in this electrolyte solution, and sonicated for 5 minutes. The mass ratio of DABA to RGO was optimized in order to get a stable dispersion with a maximum amount of RGO. It is important to mention that pH 7 is needed for these electroactive nanofluids. To adjust the pH, $LiOH{\cdot}H_2O$ was added before adding $LiFePO_4$. Finally, layered $LiFePO_4$ was added and the mixture sonicated for

35 minutes. Different amounts of RGO and $LiFePO_4$ were tested and will be discussed through the article.

The viscosity for DABA/RGO (40:1)) nanofluid is 1.055 (10) mPa·s at 20.1°C. This value is very similar to the viscosity of water at the same temperature (1.002 mPa·s). The electroactive nanofluid based on sample e $LiFePO_4$ 1.4 g/L (DABA/RGO (40:1)) has a viscosity of 1.72 mPa.s, at 20.1°C with a shear rate of 2880 s-1. This electroactive nanofluid has a higher viscosity than water and the base nanofluid, the higher viscosity is a result of the addition of the $LiFePO_4$ particles. However, this value is still reasonably low and perfectly compatible with low-energy pumping in a flow cell system.

2.4 Materials characterization

Physical Characterization. The phase purity and crystal structure of the samples were confirmed by X-ray diffraction (XRD) using PANalytical X′Pert PRO diffractometer using a Cu Kα radiation source ($\lambda = 1.5418$ Å) in the angular range $10^o \leq 2\theta \leq 70^o$ at a scan rate of 0.017^o per second. The morphology of the particles was studied by Scanning Electron Microscopy (SEM) and Transmission Electron Microscopy (TEM, Tecnai G2 F20 HRTEM) operated at an acceleration voltage of 200 keV. For TEM studies, samples were dispersed in absolute ethanol, and a drop was then put onto a holey carbon coated Cu grid and allowed to evaporate slowly under ambient conditions before being introduced for TEM characterization. Raman scattering (RS) spectra were recorded on a HORIBA Scientific LabRAM HR Raman spectrometer system using Ar laser. Rheology experiments were made in the Institute de Ciencia de Materials de Barcelona (ICMAB) with a Haake RheoStress 600.

2.5 Electrode preparation for solid-electrode test cell

The cathodes were prepared by pressing a mixture of the active materials with Carbon Super-P (Timcal) and Polyvinylidene fluoride (PVDF) binder in a weight ratio 85/10/5. They were mixed in a mortar for 5 minutes and then dispersed in N-Methyl-2-pyrrolidone and coated onto Al foil.

2.6 Solid half cells

Electrochemical test cells (Swagelok-type) were assembled in an argon-filled glove box with the coated sample electrode as working electrode, lithium metal foil as the counter/reference electrode, and 1 M solution of $LiPF_6$ in a 1:1 vol/vol mixture of ethylene carbonate and diethyl carbonate as the electrolyte. Glass microfiber filter paper was used as separator. $LiFePO_4$ solid state half cells were subject to galvanostatic charge/discharge cycles from 2.5 V to 4.0 V at different C-rates. Cyclic voltammetry was performed (1 mV/s) in the same voltage range.

2.7 Nanofluids electrochemical test

Cyclic voltammograms were carried out from -0.2 V to 1.2V vs Ag/AgCl 3.5M KCl. Pt was used as counter and working electrode during the electrochemical tests of the nanofluids. Potentiostatic electrochemical impedance spectroscopy (PEIS) experiments were carried out over a frequency range of 5000 kHz and 100000 mHz, with an amplitude of 10 mV. Before the PEIS experiments, the cell was keep at constant voltage for 10 minutes. The voltages of the experiments were 0.0 V vs. Ag/AgCl or 0.9 V vs. Ag/AgCl the electrochemical tests were carried out with a Biologic VMP3 potentiostat/galvanostat.

2.8 Electrochemical cell

A commercial Electrolysis Cell was used (BASi Bulk). A container with a porous glass frit of 4-6 μm pore diameter was used for the charge and discharge test. In the glass frit only 1.4 $g \cdot L^{-1}$ of $LiFePO_4$ DABA/RGO (40:1) nanofluid was placed. A DBA-RGO (40:1) dispersion was used as counter electrode in the 75 mL glass cell with an Ag/AgCl KCl 3.5M reference electrode immersed in it. The cell was cycled between -0.2V to 1V vs. Ag/AgCL KCl 3.5M at 1C. The dispersion was stirred during the experiment. It is important to mention that we balanced the amounts of active materials in each nanofluid electrode (1.4 $g \cdot L^{-1}$ of $LiFePO_4$ DABA/RGO (40:1) sample and the DABA/RGO (40:1) sample) to balance their charge. For instance, we then prepare a 75 mL of DABA/RGO (40:1) nanofluid and use a 1.3 mL of the $LiFePO_4$ DABA/RGO nanofluid. The calculation was based in the **Figure S2**.

3 Results

3.1 Lithium iron phosphate

The $LiFePO_4$ material prepared presents the expected olivine phase as confirmed by powder XRD (

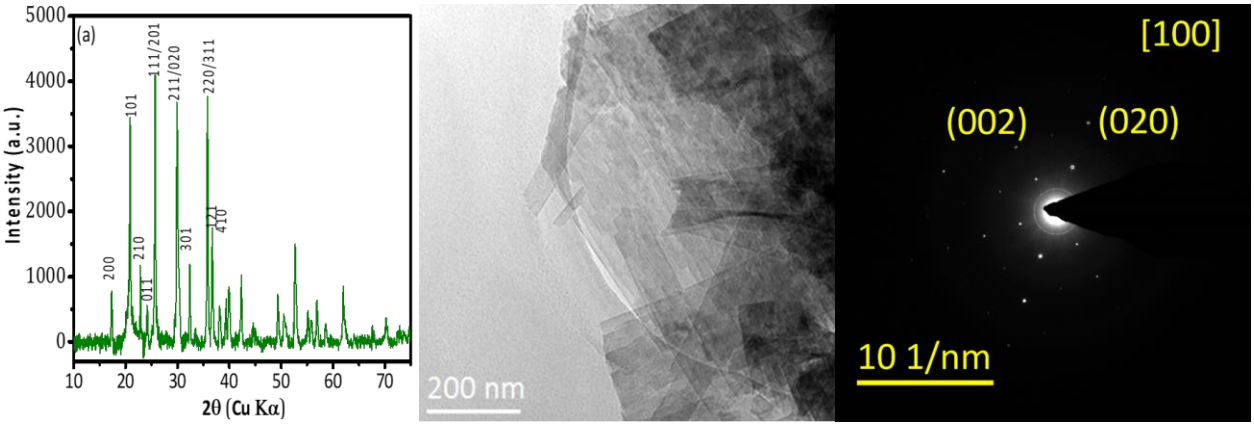

Figure 3 **a**) with high purity. All diffraction peaks are indexed to orthorhombic $LiFePO_4$ (JCPDS card number 081-1173, space group Pnma), with no impurities detected. The average primary

crystallite size, as determined from the peak width at 23 2Θ by the Scherrer equation, was 38 nm.

On the other hand, the synthesis procedure reported here for $LiFePO_4$ leads to a striking, unusual morphology and agglomeration of thin plates,

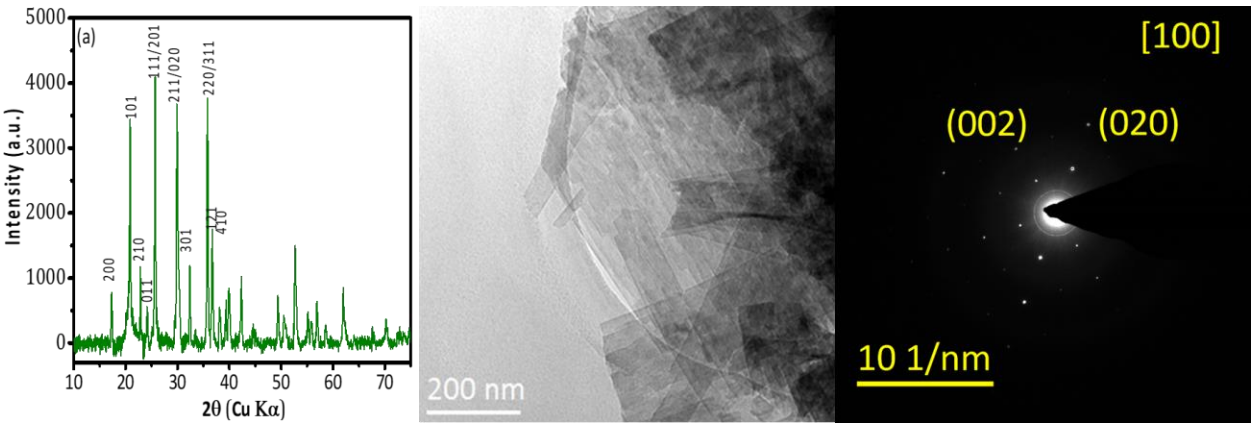

Figure 3 **b**. This sample is well crystallized, single-crystals according to their Selected Area Electron Diffraction (SAED) patterns,

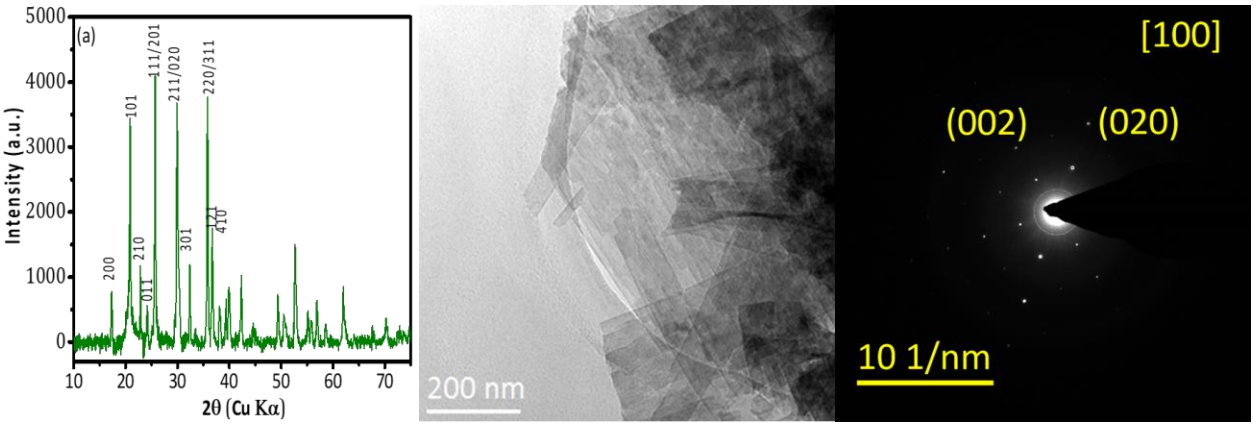

Figure 3 **c**. This analysis of the SAED pattern, obtained from the isolated nanoparticle shows in the inset of this figure, shows that this particle has a plane axis of [100]. The planes show by this nanoparticle can be index 101 and 020. These planes are listed in a JCPDS card number 081-1173 of $LIFePO_4$. Base on this information we can identify the axis of the $LiFePO_4$

nanoparticle as shows in the inset of

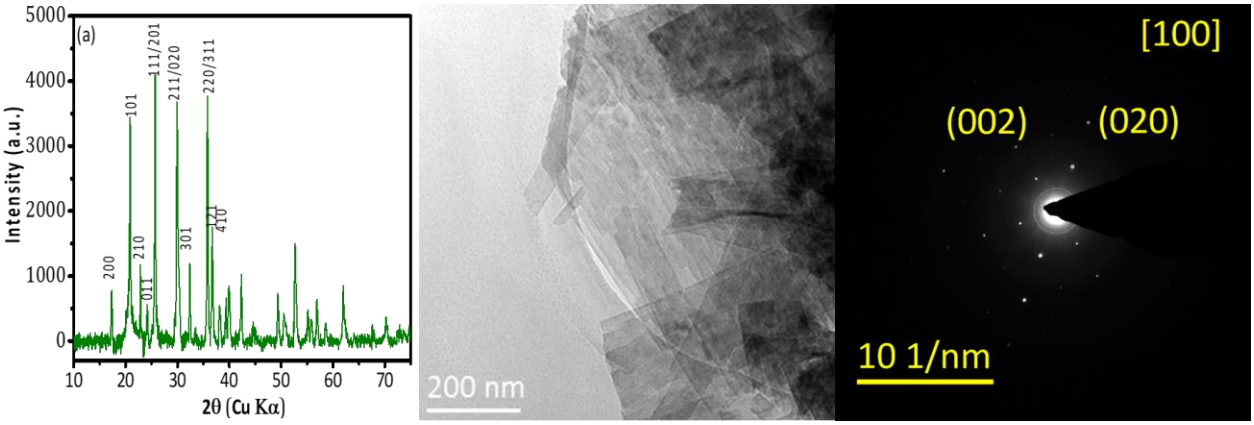

Figure 3 **c.**

The characteristic redox waves corresponding to Li ion intercalation/deintercalation can be observed in the cyclic voltammogram of pristine $LiFePO_4$ (

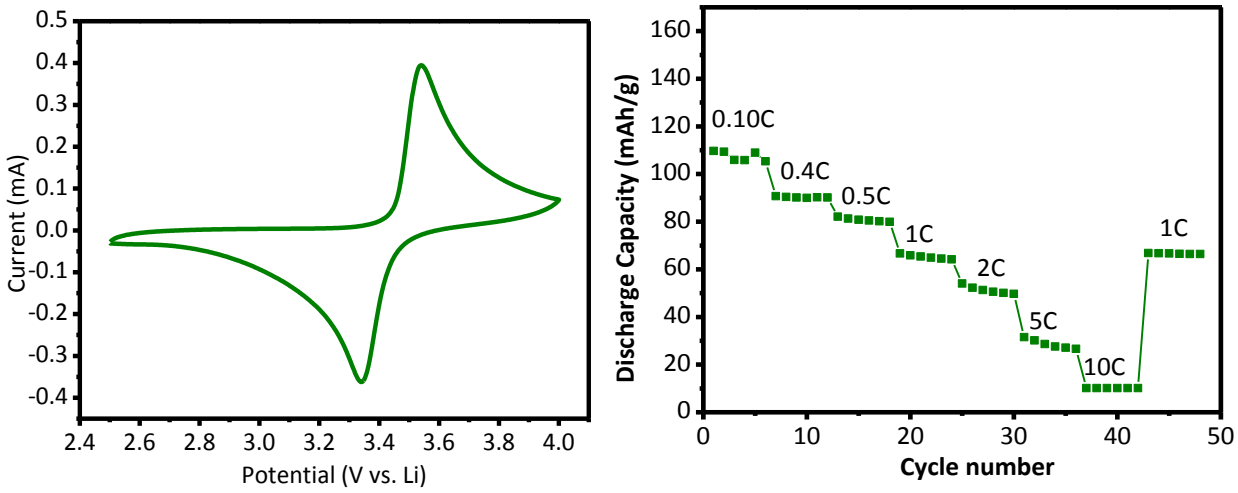

Figure 4 **a**). These peaks are broad even at 0.5 $mV \cdot s^{-1}$ and show a relatively high polarization due to the lack of a conducting coating. It is well known that $LiFePO_4$ electroactivity is hindered by its poor conductivity (10^{-9} $S \cdot cm^{-1}$) and slow lithium diffusion.[20] Increasing the conductivity

by coating the $LiFePO_4$ surface with carbon [21, 22] or conducting polymers[23, 24] have been two of the most popular approaches to improve the capacity and rate performance of $LiFePO_4$ as cathode for LIBs.

In the absence of such a conducting coating, the maximum discharge capacity obtained for this material in half cells vs. Li was around 100 $mA{\cdot}h{\cdot}g^{-1}$ at 0.10C, decreasing progressively at higher rates down to 30 $mA{\cdot}h{\cdot}g^{-1}$ at 5C and ca. 10 $mA{\cdot}h{\cdot}g^{-1}$ at 10C (

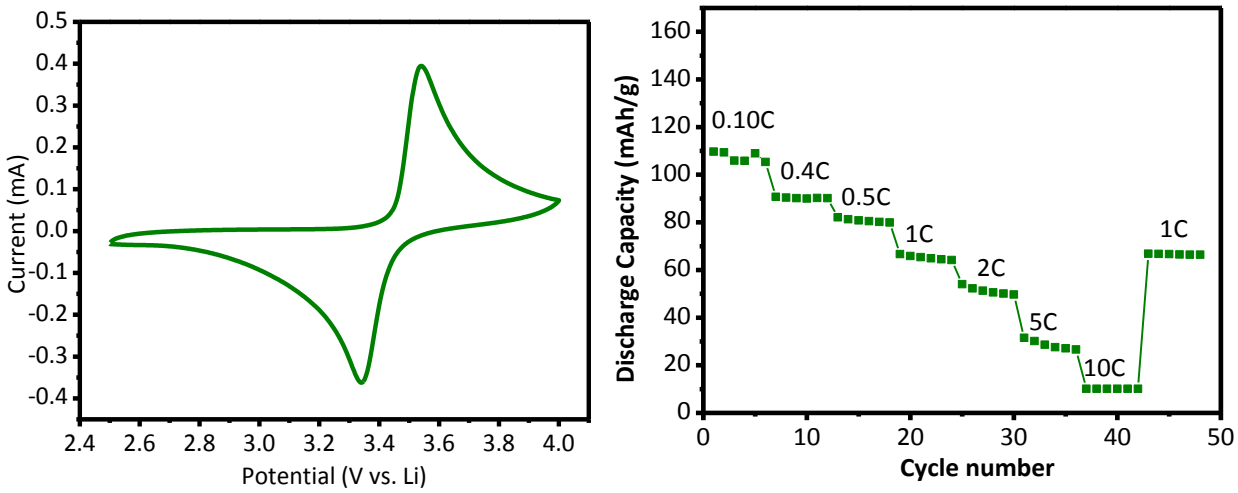

Figure 4 **b**).

3.2 RGO characterization

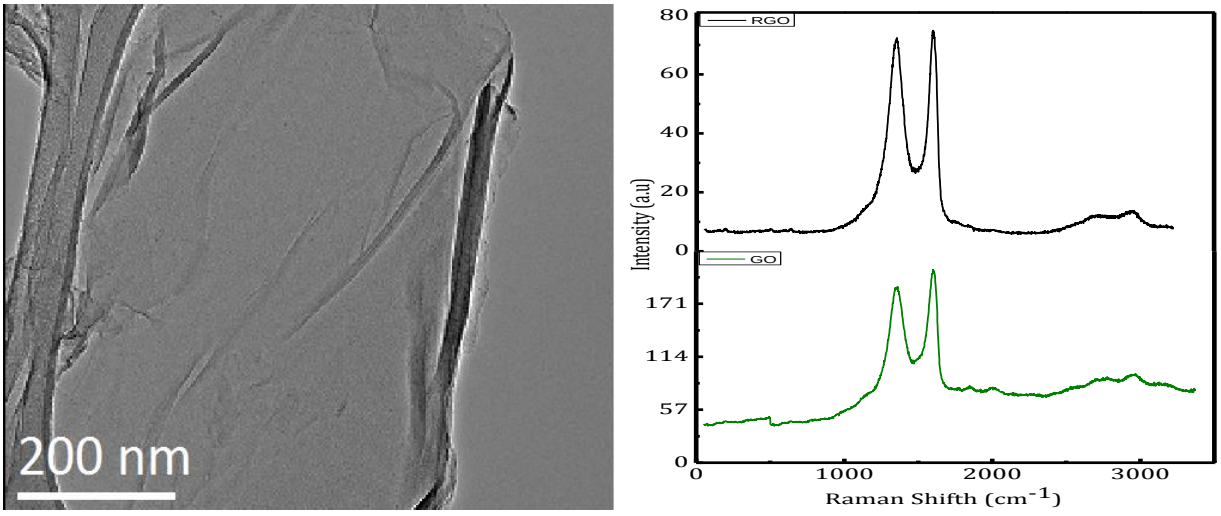

Figure 5 **a** shows micrographs of representative RGO sheets at different scales. These sheets are very thin and segregated, although their preparation for TEM results in wrinkles and partial overlap with each other. The SAED pattern of the sheet shown in the top inset (

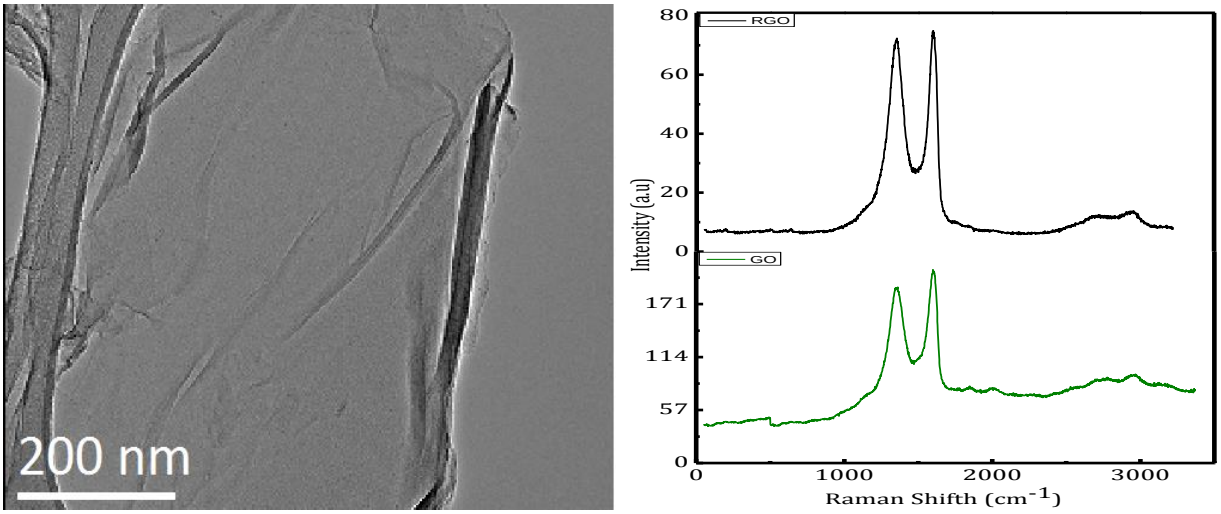

Figure 5 **a**) shows a typical hexagonal symmetry but with strongly distorted elongated spots, which is representative of single-crystalline graphene layers with a high degree of distortions.

Raman scattering is one of the most widely used techniques to characterize the structural and electronic properties of carbon materials. **Figure 3 b** shows the Raman spectrum of our RGO

with a D band at 1355.2cm^{-1} and a G band at 1595.3 cm^{-1}. The D band is related to the degree of disorder and its intensity shows the degree of edge chirality. Thus, the intensity ratio of G and D band (ID/IG) of RGO indicates the degree of the disorder. As shown in

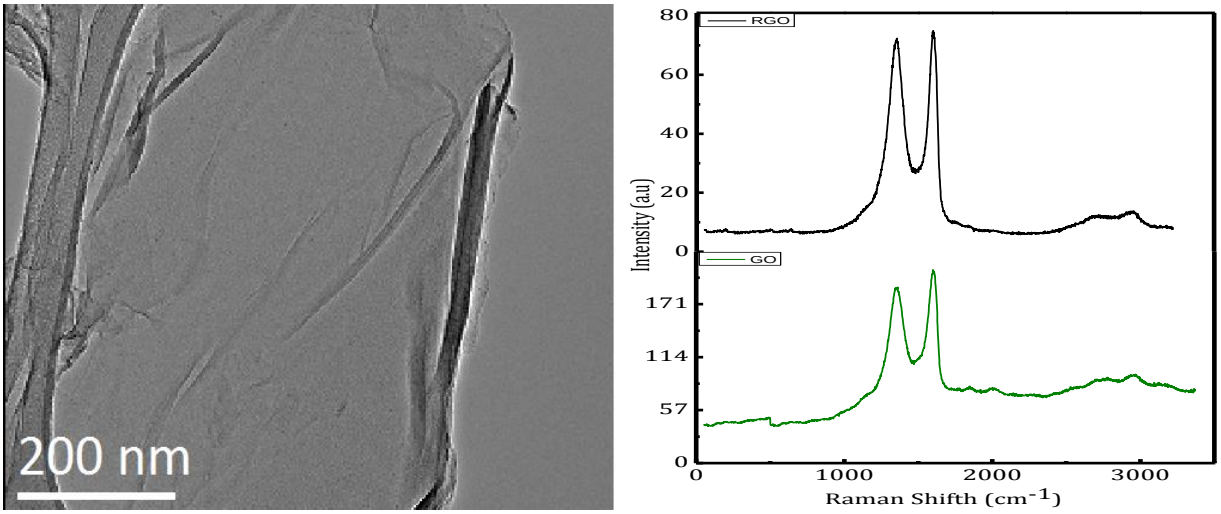

Figure 5 **b**, the ID/IG ratio of RGO is 0.99. This spectrum shows that this sample has 2 other bands at 2716.3 and 2953.9 cm^{-1}. The bands correspond to 2D (2953.9 cm^{-1}), a combination scattering peak [25, 26]; a second order overtone of a different in plane vibration D + G (2716.3 cm^{-1}).[26]

D and G Raman bands can be deconvoluted using four Gaussians or Gaussian-Lorentzian lines in order to estimate the ratio of sp^2 to sp^3 type carbon.[27] We have fitted the Raman intensity

profiles using four Gaussian lines, see 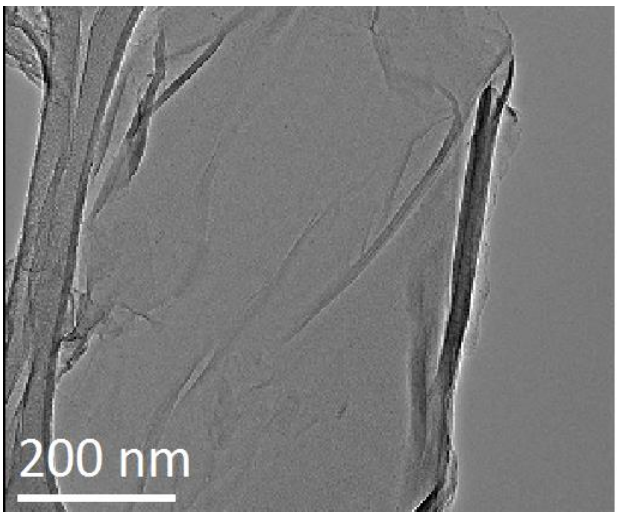

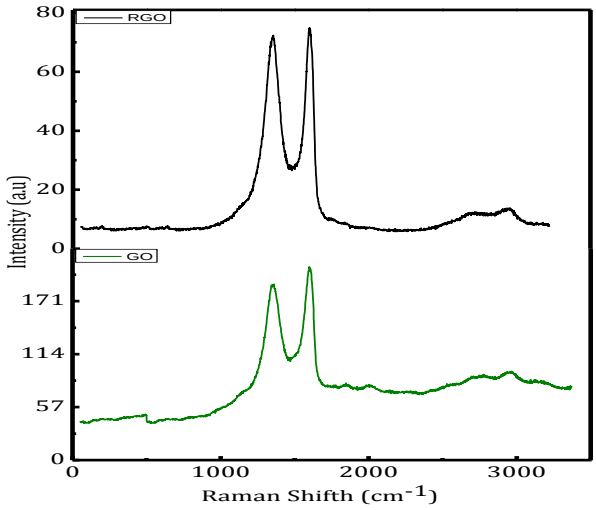

Figure 5 **b**, and have estimated intensity ratio Isp^2/Isp^3 = (I1270+ I1610) / (I1100+I1510). For RGO sample, we found a value for Isp^2/Isp^3 =3.2.

3.3 Electroactive nanofluids

Behera et al. have reported that reduced graphene oxide has a better dispersibility in a pH range of 7 to 11.[28] Guyomard and collaborators reported that $LiFePO_4$ has an initial pH near 7 in a water dispersion; they conclude that the stability and the electrochemical performance is better when the initial pH is not altered.[29] Furthermore, DABA solubility has a strong

dependence on the pH, with decreased solubilities in acidic media (**Table 1**) probably due to the protonation of its carboxylic acid moiety. Therefore, $LiOH \cdot H_2O$ was used in order to adjust the pH at 7; this compound was selected to avoid the presence of other ions in solution, see supplementary information.

As a preliminary step for the formulation of our final nanofluids, we optimized the DBA/RGO concentration in aqueous media. Three different DABA/RGO mass ratios were tested: 20:1, 30:1 and 40:1 (see

Table 3 for concentrations). As is shown in

Table 3 the more stable dispersion of DABA and RGO was the one with the mass ratio DABA/RGO 40 to 1. The stabilization of the RGO is achieved by a solvated aromatic molecule that holds back RGO in suspension by π-π interactions, the introduction of functional groups provides a steric effect that maintains the RGO layers apart.

For comparison, pure RGO was dispersed in the Li_2SO_4 aqueous electrolyte at a nominal concentration of 0.29 $g \cdot L^{-1}$. However, at this concentration RGO precipitates immediately, although a grey-colored dispersion was maintained. This means that, although some graphene flakes remain in solution thanks to the polar oxygen groups remaining in the structure of Reduced Graphene Oxide, in the absence of DABA, the solubility limit for RGO is much lower.

After DABA/RGO optimization, we proceeded to develop an electroactive nanofluid incorporating platelet $LiFePO_4$ as redox electroactive species to test the RGO/DABA dispersion.

Different amounts of $LiFePO_4$ were tested to optimize the amount of redox active material load in the nanofluid (

Table 4). The sample with 0.4 $g \cdot L^{-1}$ of $LiFePO_4$ was the most stable, however samples that contains $g \cdot L^{-1}$ and 1.4 $g \cdot L^{-1}$ of $LiFePO_4$ exhibit a stability that can be considered good enough to develop a nanofluid. Unfortunately, the sample with 2 $g \cdot L^{-1}$ of $LiFePO_4$ layer did not show good stability. Depending on the particle concentration and the strength of particle−particle interactions, a dispersion/agglomeration equilibrium is established in the particle suspension. Large concentrations of $LiFePO_4$ platelets induce agglomeration and precipitation. On the other hand, it should be noted that even gentle stirring prevents precipitation of these more concentrated nanofluids.

The electrochemical characterization of optimized nanofluids included cyclic voltammetry (CV) and impedance (PEIS) studies, as well as Galvanostatic Charge-Discharge (GCD) tests. As shown in **Fig 2 a** the CV of DABA shows an important change on its electrochemical signal when RGO is added. DABA alone did not show any special electrochemical response aside from a small capacitive signal. But the addition of RGO leads to the appearance of an oxidation wave at 0.3 V vs Ag/AgCl. Thus, RGO seems to promote an irreversible oxidation process of DABA (RGO only provide capacitive signal, inset **Fig 2 a**). This effect is associated to an improved conductivity by a percolation effect in the solution, together with the strong interaction between DABA and RGO that favors charge transfer between them. The RGO dispersion shows a capacitive behavior

rather than a faradaic redox process. DABA did not show any clear electrochemical activity beyond two very poorly defined waves.

Fig 2 b shows cyclic voltammograms of nanofluids with various $LiFePO_4$ concentrations with DABA/RGO as additive at constant concentration. They show the expected $LiFePO_4$ redox waves at 0.65 V vs Ag/AgCl and 0.19 V vs. Ag/AgCl with intensities increasing as $LiFePO_4$ concentration increases up to 1.4 $g \cdot L^{-1}$. DABA redox waves are also detected at 0.9 V vs Ag/AgCl. The sample with 1.4 $g \cdot L^{-1}$ of $LiFePO_4$ gives the best electrochemical performance, although its dispersion in the nanofluid is not as long-lasting as that of more dilute sample (i.e. 0.4 $g \cdot L^{-1}$). Thus, the 1.4 $g \cdot L^{-1}$ was further used to explore in detail the electrochemical characteristics of these nanofluids.

Fig 2 c show the electrochemical behavior of the sample at different scan rates. The intensity of the Fe(II)/Fe(III) peak corresponding to $LiFePO_4$ increases as the scan rates is increased. On the other hand, the peak corresponding to DABA appears as a shoulder at low scan rates and nearly disappears as the scan rate is increased up to 25 $mV \cdot s^{-1}$. It should be noted that the order for recording these CVs was from fastest to slowest. Thus, the disappearance of the DABA signal cannot be due to full consumption of the chemical.

This observation also depends on the amount of $LiFePO_4$, as we can see in the inset of **Fig 2 c** displaying the CV of the sample with 1 $g \cdot L^{-1}$ of $LiFePO_4$ at 25 $mV \cdot s^{-1}$, which shows a small peak that correspond to DABA oxidation. These experiments show a decrease of the DABA signal by the addition of the Fe(III)/Fe(II) redox couple ($LiFePO_4$) or an increase of the scan rate velocity. That behavior suggests that the electrochemical redox processes of $LiFePO_4$ are much faster than the oxidation of DABA, which seems to be fade in the presence of the former and at fast scan rates.

PEIS experiments were carried out for the 1.4 $g \cdot L^{-1}$ $LiFePO_4$ nanofluid and the corresponding Nyquist plots for the system in its reduced (0.0 V vs. Ag/AgCl)

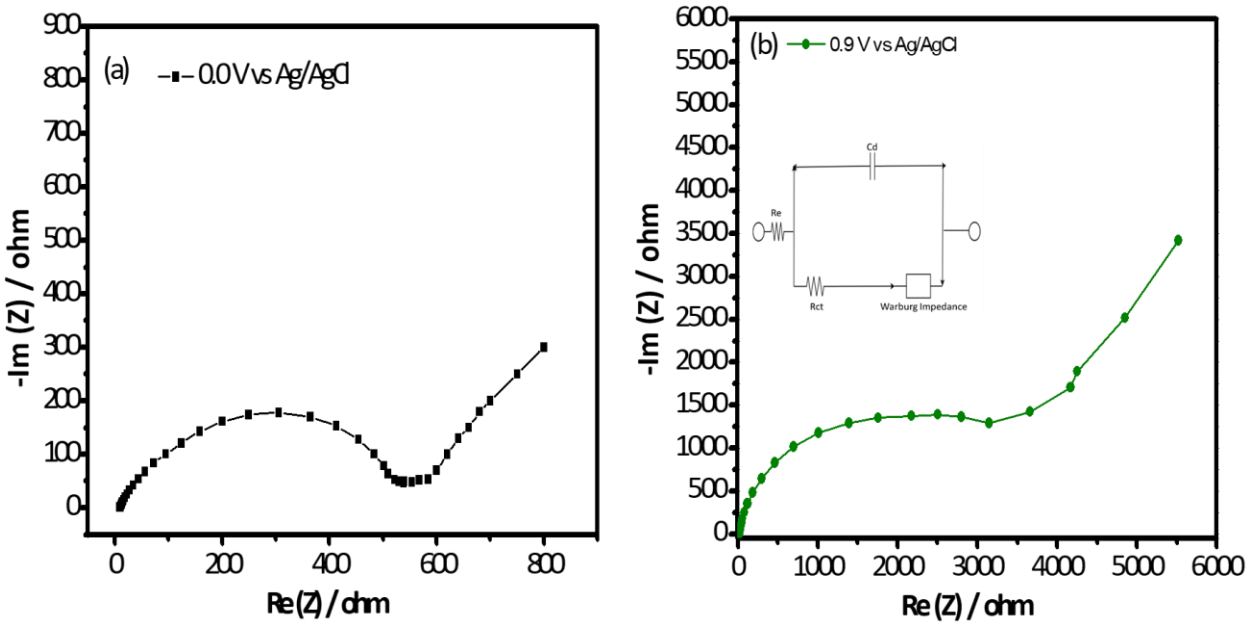

Fig 3 **a** and oxidized (0.9 V) states are shown in

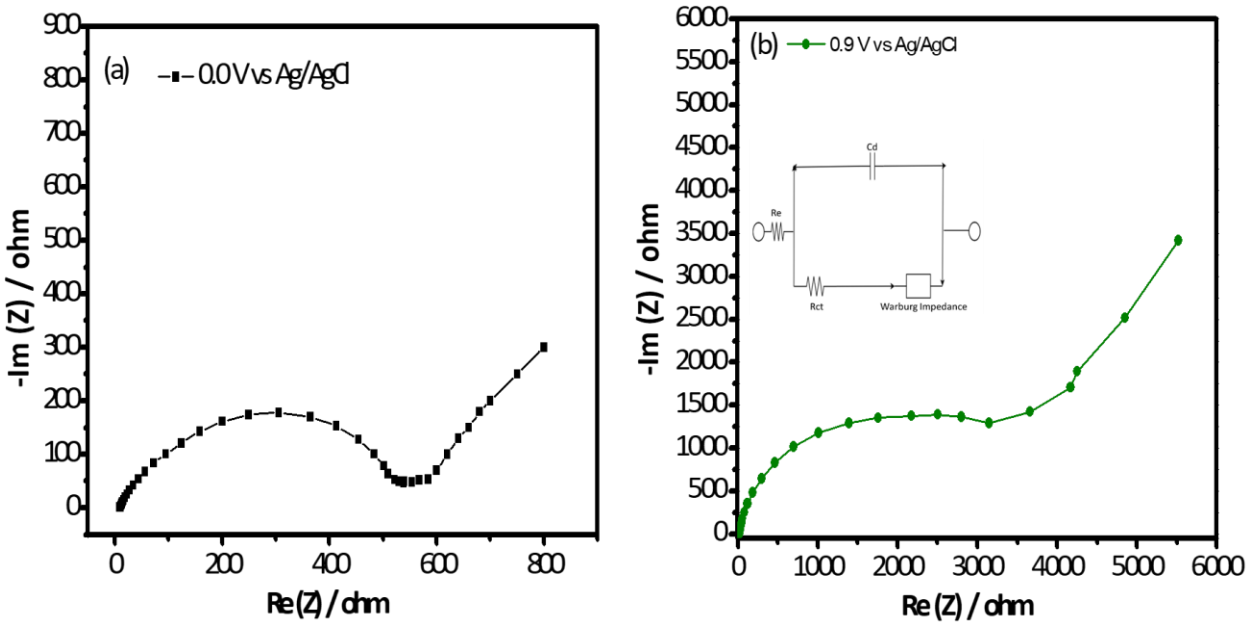

Fig 3 **b**. The results fit with the Randles equivalent circuit (inset

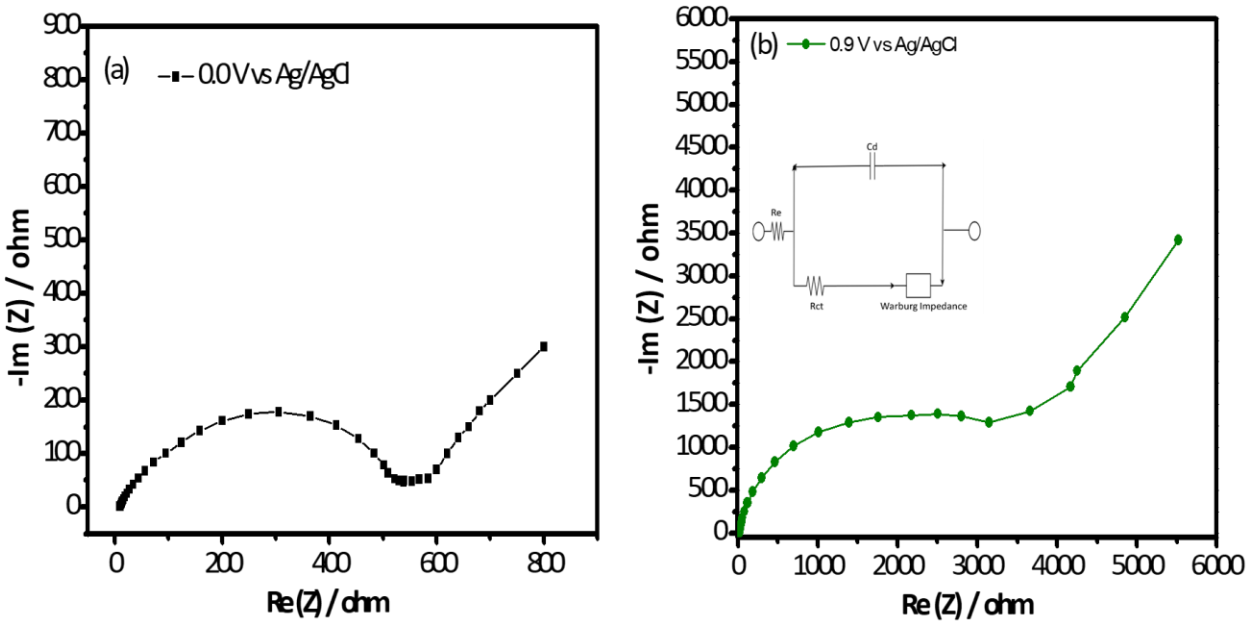

Fig 3 **b**) typical for a simple electrochemical process. In this equivalent circuit, there is a resistance associated with the electrolyte and the external circuit, which in the Nyquist plot correspond with the point in the real axes where the semicircle begins.

This point is the same for the oxidation and reduction process of the sample, the value of this resistance is negligible compare with the resistance associate with the charge transfer, discuss below.

The charge transfer resistance related to the redox process can measure by the width of the semicircle observed in the real axes of the Nyquist plot. The semicircle is larger for the oxidation than for the reduction process in $LiFePO_4$. This agree with other publications, where they found that $LiFePO_4$ is more stable than $FePO_4$[30]. This also means that the de intercalation process is less favorable than the intercalation process of $LiFePO_4$.

The inclined line in the low frequency represented the Warburg impedance (Z w), which was associated with lithium-ion diffusion of the material[31]. This process is associate with a mass transfer control.

Fig 4 **a** shows the performance of a full cell with the $LiFePO_4$ (1.4 $g \cdot L^{-1}$) -DABA/RGO (40:1) nanofluid as positive electrode and the DABA/RGO (40:1) nanofluid as negative electrode cycled at 1C. The discharge capacity of the cell is ca. 140 $mA \cdot h \cdot g^{-1}$ ($LiFePO_4$) at 1 C. This represents an improvement of ca. 37% over the solid half-cell described above making use of solid (uncoated) $LiFePO_4$ vs Li (**Fig 4 b**). In addition, the Coulombic efficiency of the cell increases continuously from 65% (1st cycle) up to ca. 90% (5th cycle). In general the results show a high utilization of the $LiFePO_4$.On the other hand, it was difficult to compare the performance of $LiFePO_4$ in an aqueous electrolyte because without the presence of RGO the Cyclic Voltammetry does not show any electrochemical signal, **Figure S3**.

Fig 4 **b** shows a plot of the potential of the working electrode vs. capacity for a single representative cycle (5th cycle). The charge capacity is larger than the discharge capacity, in agreement with the evolution of the coulombic efficiency shown in **Fig 4 a**. The profile of the cell shows a clear plateau around 0.5 V.

Fig 4 **c** shows the voltage-time profile of working and counter electrode. The working electrode shows a distorted typical profile of a voltage vs time of $LiFePO_4$. The counter electrode shows a define plateau around 0.6 V vs Ag/AgCl. The voltage time profile of the counter electrode and Figure S2 lead to a conclusion that the counter electrode storage energy base in a capacitive mechanism.

4 Conclusions.

We successfully developed a stable dispersion of RGO in water thanks to the addition of DiAminoBenzoic Aciz (DABA). This aromatic but polar molecule interacts with RGO through π-π

forces equivalent to a solvating effect. As a consequence of this interaction RGO was maintained in water as stable dispersions. Furthermore, the steric effect of the functional groups of the DABA preclude the restacking of RGO layers, which remain separated in the dispersion.

Our results demonstrate the high rate of percolation effect of the RGO/DABA nanofluid. $LiFePO_4$ nanosheets were used as a model electroactive nanoparticulate phase and showed an improvement of its redox performance. Also, our base nanofluid does not disturb the electrochemical signal of this $LiFePO_4$, despite the enhancement by RGO of a redox process of DABA (not observed with pristine DABA). The relatively much faster and reversible $LiFePO_4$ electrochemistry precludes the process of irreversible oxidation of DABA, especially at fast rates. Finally, our work shows how to harness the electroactivity of $LiFePO_4$ integrated in a freely flowing nanofluid. It should be noted that $LiFePO_4$ nanosheets in the nanofluid where not coated with any conducting material. Yet, they performed better than similarly uncoated nanoparticles integrated in a conventional solid electrode. This improved performance must be assigned to the efficient charge-transfer from current collectors mediated by RGO in the nanofluid.

We hope that these results could help to establish a new path for the development of high energy density electroactive fluids with low viscosities that can be applied in a new generation of flow cells.

Supporting Information

Supporting Information is available from the Wiley Online Library or from the author.

Acknowledgements

Partial funding from the Spanish MINECO MAT2015-68394-R (NaCarFLOW) and

AGAUR Generalitat de Catalunya 2014_SGR_1505 Proyecto NESTOR is aknowledged.

References

[1] Q. Huang, Q. Wang, Next-Generation, High-Energy-Density Redox Flow Batteries, ChemPlusChem, 80 (2015) 312-322.

[2] G.L. Soloveichik, Flow Batteries: Current Status and Trends, Chem. Rev., 115 (2015) 11533-11558.

[3] Z. Yang, J. Zhang, M.C.W. Kintner-Meyer, X. Lu, D. Choi, J.P. Lemmon, J. Liu, Electrochemical Energy Storage for Green Grid, Chem. Rev., 111 (2011) 3577-3613.

[4] M. Duduta, B. Ho, V.C. Wood, P. Limthongkul, V.E. Brunini, W.C. Carter, Y.-M. Chiang, Semi-Solid Lithium Rechargeable Flow Battery, Advanced Energy Materials, 1 (2011) 511-516.

[5] V. Presser, C.R. Dennison, J. Campos, K.W. Knehr, E.C. Kumbur, Y. Gogotsi, The Electrochemical Flow Capacitor: A New Concept for Rapid Energy Storage and Recovery, Advanced Energy Materials, 2 (2012) 895-902.

[6] S. Sasi, A. Murali, S.V. Nair, A.S. Nair, K.R.V. Subramanian, The effect of graphene on the performance of an electrochemical flow capacitor, Journal of Materials Chemistry A, 3 (2015) 2717-2725.

[7] M. Boota, K.B. Hatzell, M. Alhabeb, E.C. Kumbur, Y. Gogotsi, Graphene-containing flowable electrodes for capacitive energy storage, Carbon, 92 (2015) 142-149.

[8] S. Hamelet, T. Tzedakis, J.-B. Leriche, S. Sailler, D. Larcher, P.-L. Taberna, P. Simon, J.-M. Tarascon, Non-Aqueous Li-Based Redox Flow Batteries, J. Electrochem. Soc., 159 (2012) A1360-A1367.

[9] L. Madec, M. Youssry, M. Cerbelaud, P. Soudan, D. Guyomard, B. Lestriez, Surfactant for Enhanced Rheological, Electrical, and Electrochemical Performance of Suspensions for Semisolid Redox Flow Batteries and Supercapacitors, ChemPlusChem, 80 (2015) 396-401.

[10] M. Boota, K.B. Hatzell, M. Beidaghi, C.R. Dennison, E.C. Kumbur, Y. Gogotsi, Activated Carbon Spheres as a Flowable Electrode in Electrochemical Flow Capacitors, J. Electrochem. Soc., 161 (2014) A1078-A1083.

[11] J.W. Campos, M. Beidaghi, K.B. Hatzell, C.R. Dennison, B. Musci, V. Presser, E.C. Kumbur, Y. Gogotsi, Investigation of carbon materials for use as a flowable electrode in electrochemical flow capacitors, Electrochim. Acta, 98 (2013) 123-130.

[12] Q. Huang, H. Li, M. Gratzel, Q. Wang, Reversible chemical delithiation/lithiation of LiFePO4: towards a redox flow lithium-ion battery, PCCP, 15 (2013) 1793-1797.

[13] S. Sen, V. Govindarajan, C.J. Pelliccione, J. Wang, D.J. Miller, E.V. Timofeeva, Surface Modification Approach to TiO2 Nanofluids with High Particle Concentration, Low Viscosity, and Electrochemical Activity, ACS Applied Materials & Interfaces, 7 (2015) 20538-20547.

[14] D.P. Dubal, P. Gomez-Romero, Electroactive graphene nanofluids for fast energy storage, 2D Materials, 3 (2016) 031004.

[15] L. Xu, J.-W. McGraw, F. Gao, M. Grundy, Z. Ye, Z. Gu, J.L. Shepherd, Production of High-Concentration Graphene Dispersions in Low-Boiling-Point Organic Solvents by Liquid-Phase Noncovalent Exfoliation of Graphite with a Hyperbranched Polyethylene and Formation of Graphene/Ethylene Copolymer Composites, The Journal of Physical Chemistry C, 117 (2013) 10730-10742.

[16] H. Wei, Y.-Y. Li, J. Chen, Y. Zeng, G. Yang, Y. Li, Dispersion of Reduced Graphene Oxide in Multiple Solvents with an Imidazolium-Modified Hexa-peri-hexabenzocoronene, Chemistry – An Asian Journal, 7 (2012) 2683-2689.

[17] A.K. Padhi, K.S. Nanjundaswamy, J.B. Goodenough, Phospho-olivines as Positive-Electrode Materials for Rechargeable Lithium Batteries, J. Electrochem. Soc., 144 (1997) 1188-1194.

[18] J. Hassoun, F. Bonaccorso, M. Agostini, M. Angelucci, M.G. Betti, R. Cingolani, M. Gemmi, C. Mariani, S. Panero, V. Pellegrini, B. Scrosati, An Advanced Lithium-Ion Battery Based on a Graphene Anode and a Lithium Iron Phosphate Cathode, Nano Lett., 14 (2014) 4901-4906.

[19] W.S. Hummers, R.E. Offeman, Preparation of Graphitic Oxide, J. Am. Chem. Soc., 80 (1958) 1339-1339.

[20] Y.-N. Xu, S.-Y. Chung, J.T. Bloking, Y.-M. Chiang, W.Y. Ching, Electronic Structure and Electrical Conductivity of Undoped $LiFePO_4$, Electrochem. Solid-State Lett., 7 (2004) A131-A134.

[21] N. Ravet, Y. Chouinard, J.F. Magnan, S. Besner, M. Gauthier, M. Armand, Electroactivity of natural and synthetic triphylite, J. Power Sources, 97–98 (2001) 503-507.

[22] Z. Cabán-Huertas, O. Ayyad, D.P. Dubal, P. Gómez-Romero, Aqueous synthesis of $LiFePO_4$ with Fractal Granularity, Scientific Reports, 6 (2016) 27024.

[23] A. Fedorková, A. Nacher-Alejos, P. Gómez-Romero, R. Oriňáková, D. Kaniansky, Structural and electrochemical studies of PPy/PEG-$LiFePO_4$ cathode material for Li-ion batteries, Electrochim. Acta, 55 (2010) 943-947.

[24] A.V. Murugan, T. Muraliganth, A. Manthiram, Microwave-Irradiated Solvothermal Synthesis of $LiFePO_4$ Nanorods and their Nanocomposites for Lithium Ion Batteries, ECS Transactions, 16 (2009) 49-56.

[25] R. Saito, A. Jorio, A.G. Souza Filho, G. Dresselhaus, M.S. Dresselhaus, M.A. Pimenta, Probing Phonon Dispersion Relations of Graphite by Double Resonance Raman Scattering, Phys. Rev. Lett., 88 (2001) 027401.

[26] R. Saito, M. Hofmann, G. Dresselhaus, A. Jorio, M.S. Dresselhaus, Raman spectroscopy of graphene and carbon nanotubes, Adv. Phys., 60 (2011) 413-550.

[27] N.J. Dudney, Thin Film Micro-Batteries, Electrochem. Soc. Interface, 17 (2008).

[28] S. Kashyap, S. Mishra, S.K. Behera, Aqueous Colloidal Stability of Graphene Oxide and Chemically Converted Graphene, Journal of Nanoparticles, 2014 (2014) 6.

[29] W. Porcher, P. Moreau, B. Lestriez, S. Jouanneau, D. Guyomard, Is LiFePO4 Stable in Water?: Toward Greener Li–Ion Batteries, Electrochem. Solid-State Lett., 11 (2008) A4-A8.

[30] P. Tang, N.A.W. Holzwarth, Y.A. Du, Comparison of the electronic structures of four crystalline phases of FePO4, Physical Review B, 76 (2007) 174118.

[31] A. Fedorkova, R. Orinakova, A. Orinak, M. Kupkova, H.D. Wiemhofer, J.N. Audinot, J. Guillot, Electrochemical and XPS study of LiFePO4 cathode nanocomposite with PPy/PEG conductive network, Solid State Sciences, 14 (2012) 1238-1243.

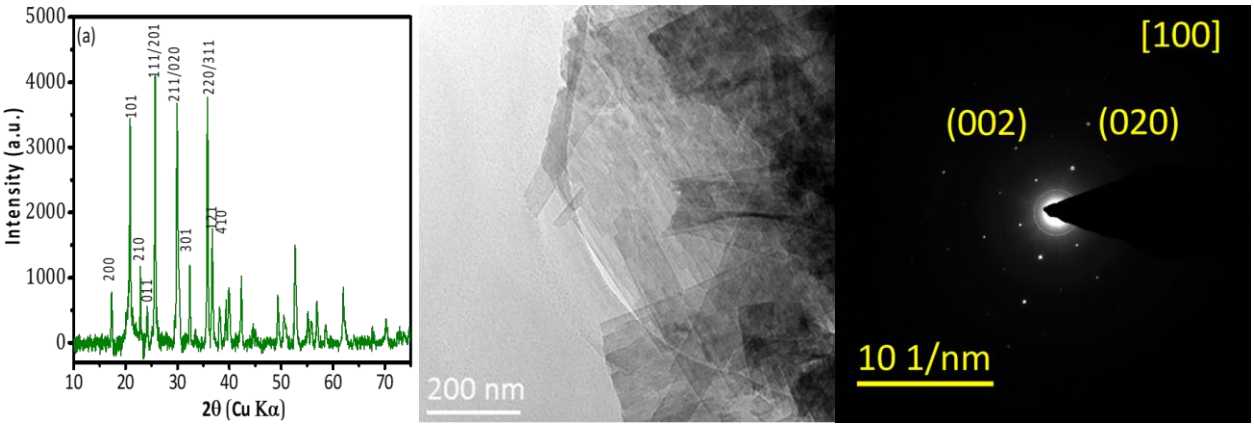

Figure 1 (a) XRD pattern (indexes shown only up to 37º) (b) TEM image showing the flake microstructure and (c) Selected Area Electron Diffraction (SAED) pattern; all corresponding to our solid $LiFePO_4$ material.

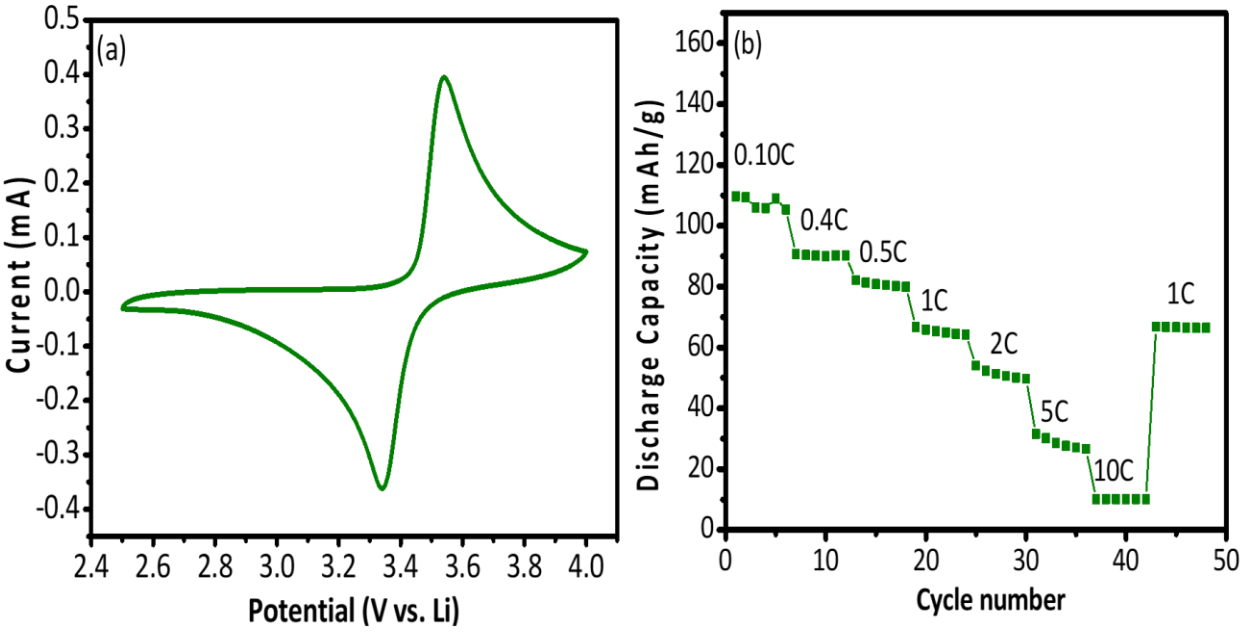

Fig 1 (a) Cyclic Voltammetry of $LiFePO_4$ scan rate 0.5 $mV \cdot s^{-1}$ (b) Rate Capability of the half-cell $Li/LiFePO_4$ from Galvanostatic Charge-Discharge measurements at various current densities.

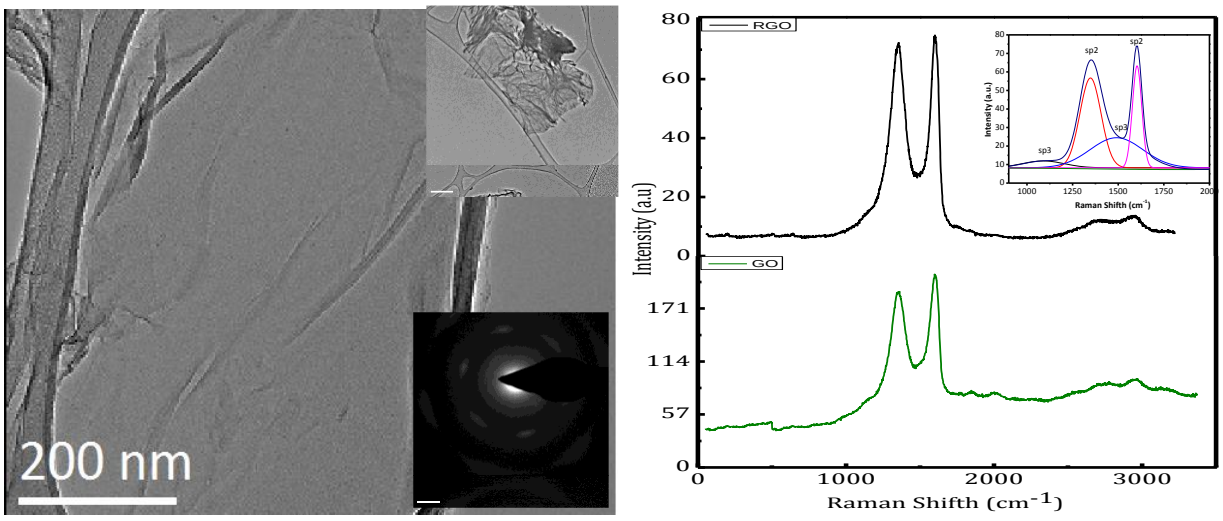

Figure 2 (a) RGO HRTEM image, inset SAED and TEM image (b) Raman spectra of GO (bottom) and RGO (top) (inset shows RGO D and G band deconvolution)

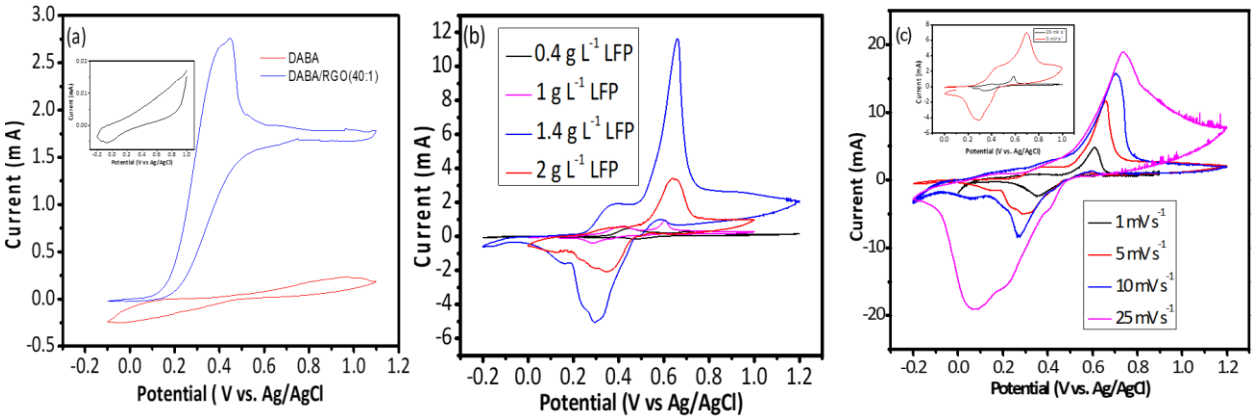

Fig 2 (a) Cyclic Voltammograms of DABA (12 g L^{-1}) (red trace) and DABA/RGO (12 g L^{-1} and 0.3 g L^{-1} respectively) (blue) showing a characteristic irreversible oxidation wave of DABA enabled by RGO. Scan rate 5 mV s^{-1} (b) Cyclic Voltammograms of $LiFePO_4$ (DABA-RGO (40/1)) (concentrations of $LiFePO_4$ 0.4 g L^{-1}, 1 g L^{-1}, 1.4 g L^{-1}, 2 g L^{-1}). Scan rate 5 mV s^{-1}. (c) Cyclic Voltammetry at different scan rates of $LiFePO_4$ (1.4 g L^{-1}). Inset shows the CV of a 1g L^{-1} $LiFePO_4$ in DABA/RGO (40/1) in which the characteristic wave from DABA is still apparent.

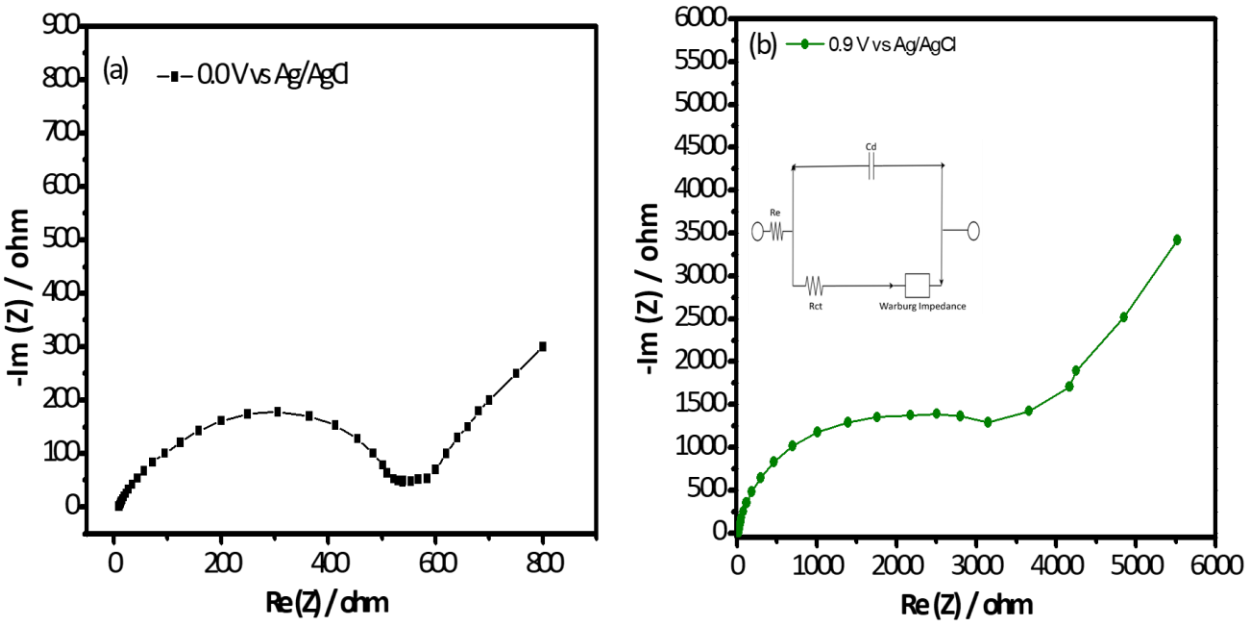

Fig 3 PEIS impedance spectra of $LiFePO_4$ (1.4 g L^{-1}) in DABA/RGO (40:1) (a) recorded at 0.0V (reduced) and (b) at 0.9 V (oxidized).

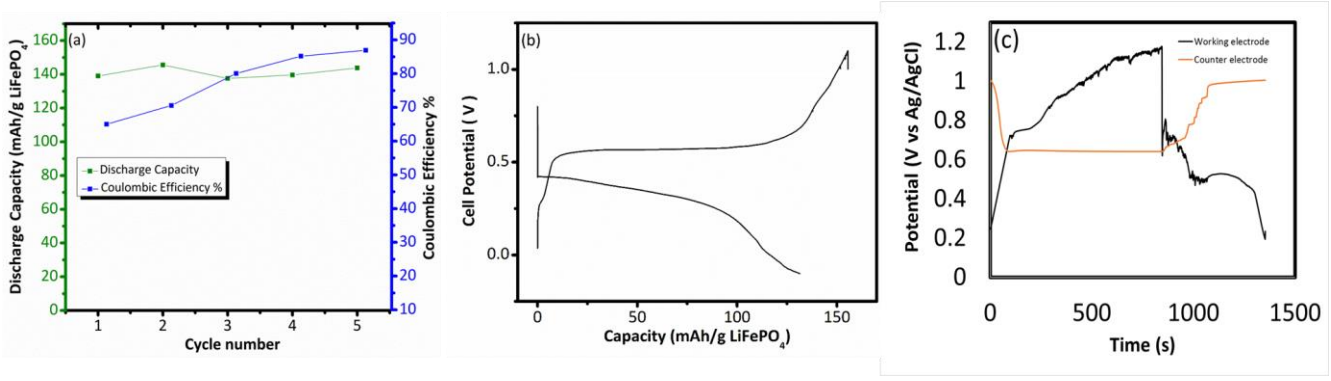

Fig 4 (a) Evolution of discharge capacity and coulombic efficiency of a two-nanofluid cell with $LiFePO_4$(1.4 g L^{-1})-DABA/RGO (40/1) as positive and DABA/RGO (40/1) as negative electrodes. Full cell cycled at 1C. (b) Charge and Discharge profiles (cell Voltage vs. charge) of the full Nanofluids cell (c) Profiles of both nanofluid electrodes (Potential vs. time).

Table 1 DABA experimental solubility

DABA concentration	$LiOH.H_2O$	pH	Solubility
12 g/L	N/A	4	no
12 g/L	1.6 g/L	6	partially
12 g/L	2.8 g/L	7	yes
12 g/L	3.6 g/L	10	yes

Table 2 Stability of the nanofluids (12 mg/mL DABA, 2.8 mg/mL $LiOH.H_2O$, 1M of $Li_2SO_4 \cdot H_2O$, pH 7)

Sample	Time (hours)	Opacity	Precipitation
Diaminobenzoic acid / RGO (20:1) (0.6g/L RGO)	7	Translucent	Precipitation star at 4 hrs.
Diaminobenzoic acid / RGO (30:1) (0.4 g/L RGO)	56	(orange) Decrease with time	Precipitation star at 27 hrs.
Diaminobenzoic acid / RGO (40:1) (0.3 g/LRGO)	120	(orange) Decrease with time	Precipitation star at 97 hrs.
Triton x (0.100 mL) 0.3 g/L Super P	5	Black	Start at 2 hours
Diaminobenzoic acid / RGO (40:1)/ 0.4 g/L $LiFePO_4$	36	Brown color	Precipitation star around 24 hours
Diaminobenzoic acid / RGO (40:1)/ 1 g/L $LiFePO_4$	Around 24	Almost Black	N/A
Diaminobenzoic acid / RGO (40:1)/ 1.4 g/L $LiFePO_4$	Around 24	Almost black	N/A
Diaminobenzoic acid / RGO (40:1)/ 2 g/L $LiFePO_4$	More than 12 less than 24	Black	N/A
Triton x (0.100 mL) Super P (0.3 g/L) $LiFePO_4$ (1.4 g/L)	6	Black	Precipitation star at 30 minutes.

Figures

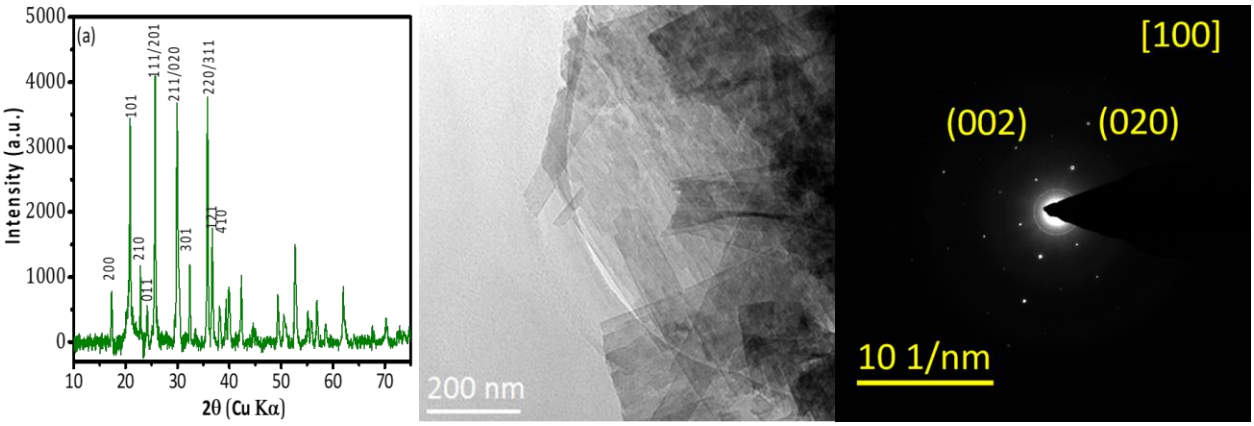

Figure 3 (a) XRD pattern of $LiFePO_4$ (b) TEM images of $LiFePO_4$ inset SAED picture and HRTEM)

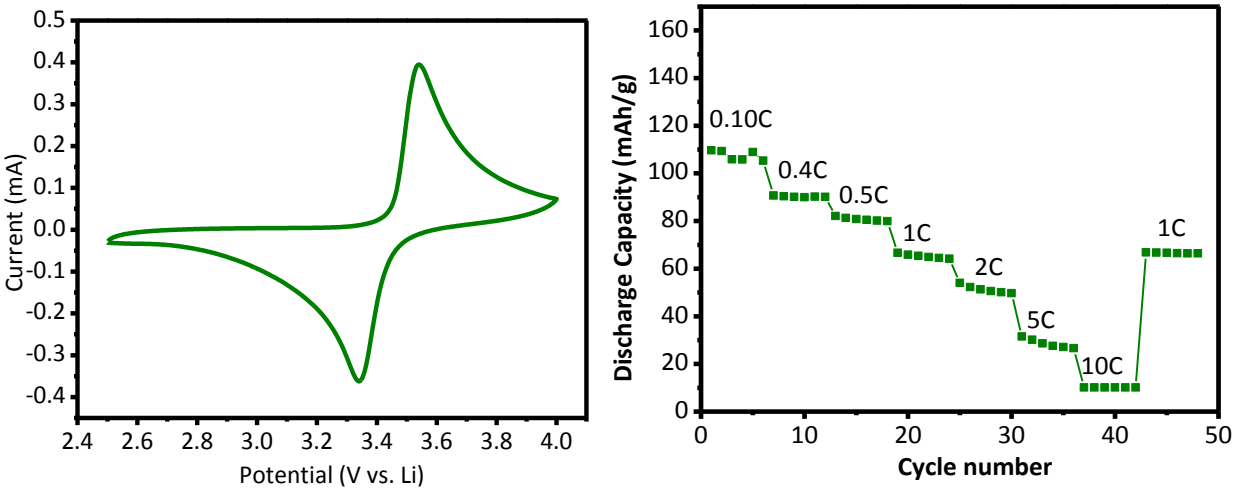

Figure 4 (a) Cyclic Voltammetry of $LiFePO_4$ scan rate 0.5 $mV \cdot s^{-1}$ (b) Rate Capability of the half-cell Li/$LiFePO_4$ (solid electrodes) from Galvanostatic Charge-Discharge measurements at various current densities.

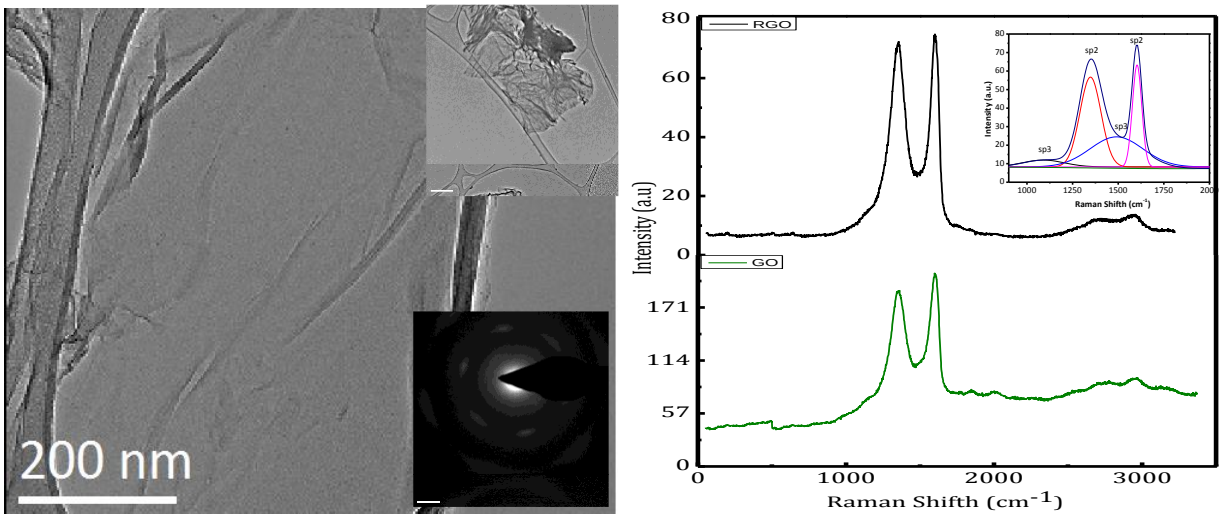

Figure 5 (a) RGO HRTEM image, inset SAED and TEM image (b) Raman spectra of GO and RGO (inset RGO D and G band deconvolution)

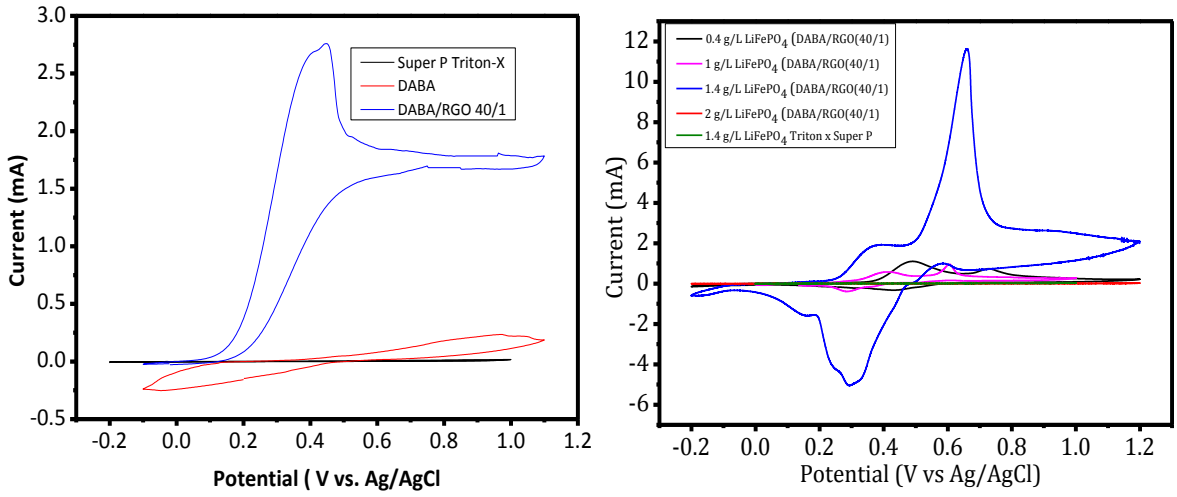

Figure 6 (a) Cyclic Voltammograms of DABA (12 g L^{-1}) (red trace) and DABA/RGO (12 g L^{-1} and 0.3 g L^{-1} respectively) (blue) showing a characteristic irreversible oxidation wave of DABA enabled by RGO. Scan rate 5 mV s^{-1} (b) Cyclic Voltammograms of $LiFePO_4$ (DABA-RGO (40/1)) (concentrations of $LiFePO_4$ 0.4 g L^{-1}, 1 g L^{-1}, 1.4 g L^{-1}, 2 g L^{-1}). Scan rate 5 mV s^{-1}. c Cyclic Voltammetry at different scan rates of $LiFePO_4$ (1.4 g L^{-1}). Inset shows the CV of a 1g L^{-1} $LiFePO_4$ in DABA/RGO (40/1) in which the characteristic wave from DABA is still apparent.

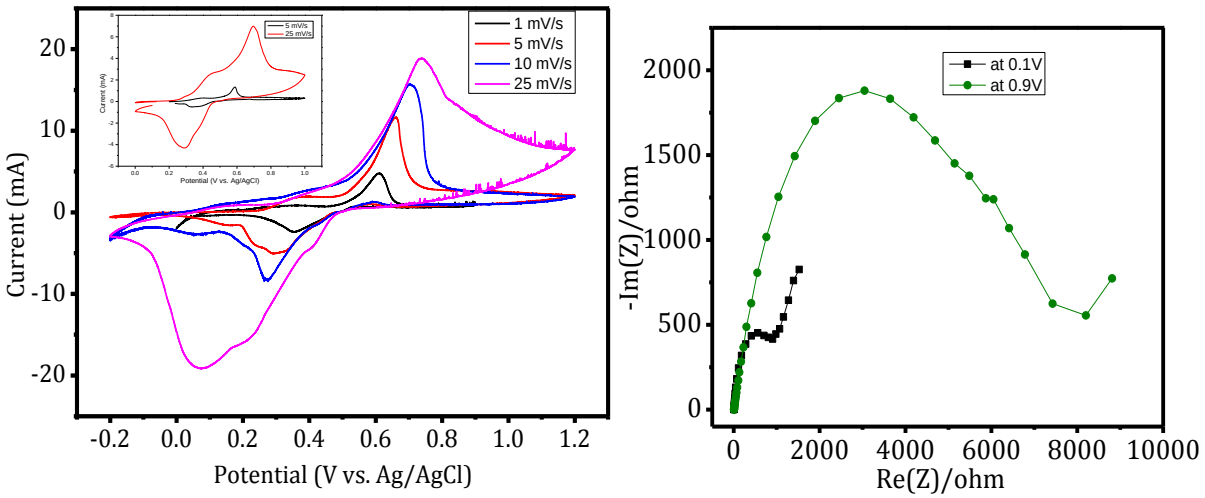

Figure 7. Left: Cyclic Voltammetry at different scan rates of the nanofluid with 1.4 g/L of $LiFePO_4$ in DABA/RGO (40:1). Inset CV of 1g/L $LiFePO_4$ in DABA/RGO (40:1). Right: AC impedance of a nanofluid with 1.4 g/L of $LiFePO_4$ in DABA/RGO (40:1). Recorded at 0.1V (reduced) and at 0.9 V (oxidized) vs Ag/AgCl.

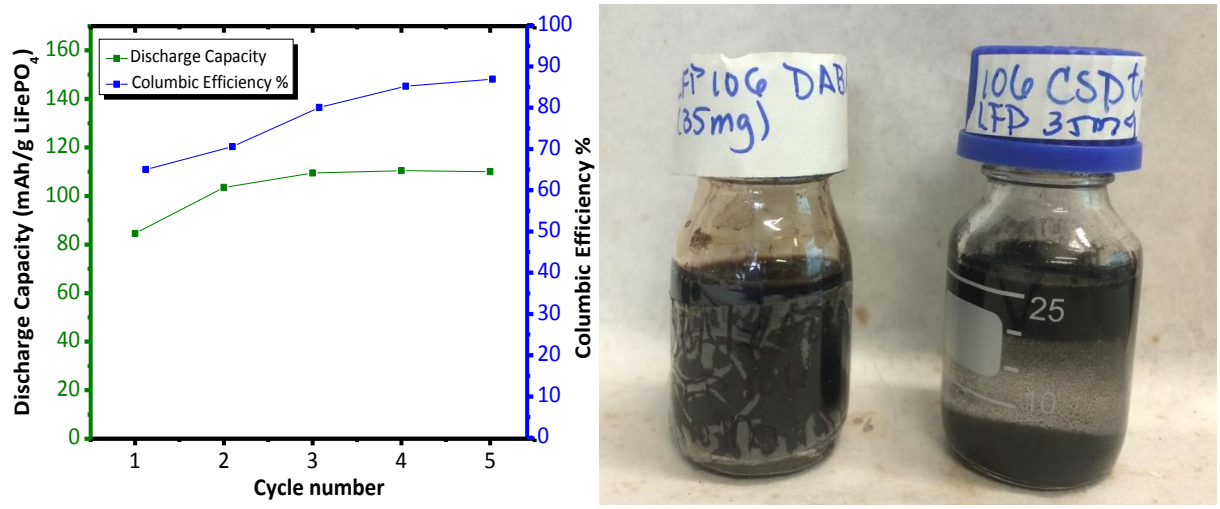

Figure 8 Evolution of discharge capacity and coulombic efficiency of a two-nanofluid full cell with $LiFePO_4$ (1.4 g L^{-1})-DABA/RGO (40/1) as positive and DABA/RGO (40/1) as negative electrodes. Full cell cycled at 1C.

. (b) 1.4 g/L of $LiFePO_4$ DABA/RGO (40:1) solution and Triton x (0.100 mL) Super P (3 g/L) $LiFePO_4$ (1.4 g/L) solution.

Tables

Table 3 DABA experimental solubility

DABA concentration	$LiOH.H_2O$	pH	Solubility
12 $g \cdot L^{-1}$	N/A	4	no
12 $g \cdot L^{-1}$	1.6 $g \cdot L^{-1}$	6	partially
12 $g \cdot L^{-1}$	2.8 $g \cdot L^{-1}$	7	yes
12 $g \cdot L^{-1}$	3.6 $g \cdot L^{-1}$	10	yes

Table 4 Stability of the nanofluids (12 mg/mL DABA, 2.8 mg/mL $LiOH.H_2O$, 1M of $Li_2SO_4 \cdot H_2O$, pH 7)

Sample	Time (hours)	Aspect	Precipitation
Diaminobenzoic acid / RGO (20:1) (0.6 $g \cdot L^{-1}$ RGO)	7	Translucent	Precipitation starts after 4 hrs.
Diaminobenzoic acid / RGO (30:1) (0.4 $g \cdot L^{-1}$ RGO)	56	(orange) Decrease with time	Precipitation starts after 27 hrs.
Diaminobenzoic acid / RGO (40:1) (0.3 $g \cdot L^{-1}$ RGO)	120	(orange) Decrease with time	Precipitation starts after 97 hrs.
RGO (0.29 g/L)	N/A	Translucent grey	immediate
Diaminobenzoic acid / RGO (40:1)/ 0.4 $g \cdot L^{-1}$ $LiFePO_4$	36	Brown color	Precipitation starts after ca. 24 hours
Diaminobenzoic acid / RGO (40:1)/ 1 $g \cdot L^{-1}$ $LiFePO_4$	Around 24	Almost Black	N/A
Diaminobenzoic acid / RGO (40:1)/ 1.4 $g \cdot L^{-1}$ $LiFePO_4$	Around 24	Almost black	N/A
Diaminobenzoic acid / RGO (40:1)/ 2 $g \cdot L^{-1}$ $LiFePO_4$	More than 12 less than 24	Black	N/A
Triton x 100 (12 $g \cdot L^{-1}$) and SuperP 0.3 g/L $LiFePO_4$ (1.4 $g \cdot L^{-1}$)	6	Black	Precipitation starts after 30 minutes.